Hidden message: looking for attenuation proxy in optical observations

Kasia Małek*

Junais, Agnieszka Pollo, Misha Hamed, Gabriele Riccio, Krzysiek Lisiecki, Patryk Matera and others




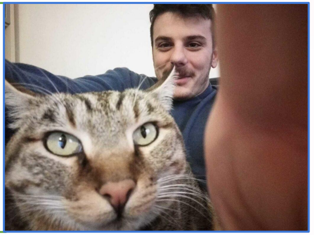
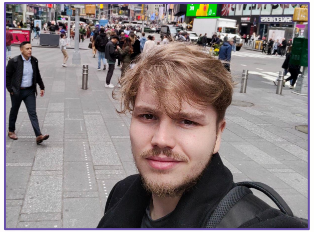
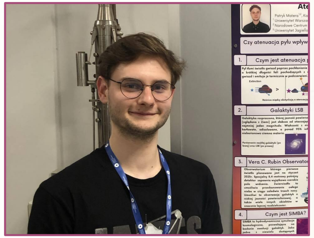

National Science Centre

National Centre for Nuclear Research Świerk

MOTIVATION

Determination of a galaxy's **star formation rate** (SFR) and **stellar mass**, also for low surface brightness galaxies (LSBs), is critical for the studies of galaxy evolution.

SFR indicators proposed and utilised over the years are based on the:

- nebular line emission (i.e. Hα, Hβ, OII), and

Lamareille+2006

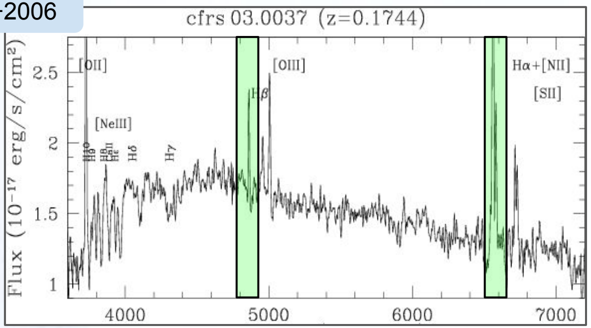

MOTIVATION

Determination of a galaxy's **star formation rate** (SFR) and **stellar mass**, also for LSBs, is critical for the studies of galaxy evolution.

SFR indicators proposed and utilised over the years are based on the:

- nebular line emission (i.e. Hα, Hβ, OII), and
- the stellar continuum emission

  (spectral energy distribution - SED - modelling)

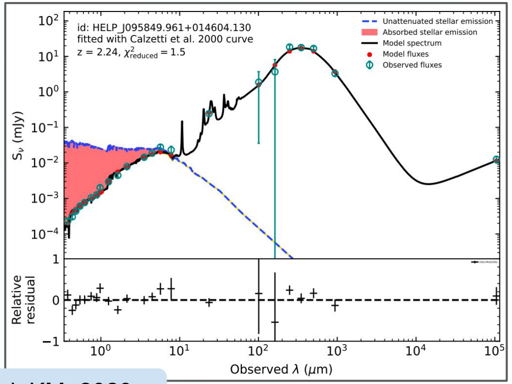

Hamed, KM+2023

MOTIVATION

Determination of a galaxy's **star formation rate** (SFR) and **stellar mass**, also for LSBs, is critical for the studies of galaxy evolution.

SFR indicators proposed and utilised over the years are based on the:

- nebular line emission (i.e. Hα, Hβ, OII), and
- the stellar continuum emission (i.e. SED - modelling)
- SFR calibrators for star forming galaxies

Brown et al. (2017) – *GALEX*-SDSS DR3 (66 nearby galaxies at $D < 10$ Mpc) – Kroupa IMF

$$\log(\mathrm{SFR})(M_\odot\ \mathrm{yr}^{-1}) = \frac{f - B}{A} - 1.26 \tag{B.1}$$

$$f = \log(L_{FUV}) + 2(M_{FUV} - M_{NUV}) \text{ with } A = 0.9 \text{ and } B = 42.25 \quad \text{[Calzetti et al. (2000) attenuation law]} \tag{B.2}$$

$$f = \log(L_{FUV}) + 1.532(M_{FUV} - M_{NUV}) - 0.033 \text{ with } A = 0.96 \text{ and } B = 42.42 \quad \text{[Hao et al. (2011) attenuation law]} \tag{B.3}$$

Davies et al. (2016) – GAMA II survey (3749 galaxies at $z < 0.13$) – Chabrier IMF

$$\log(SFR_{NUV})\ (M_\odot\ \mathrm{yr}^{-1}) = 0.62 \times (\log[L_{NUV}(\mathrm{W\ Hz}^{-1})] - 21.5) + 0.014 \tag{B.4}$$

$$\log(SFR_{FUV})\ (M_\odot\ \mathrm{yr}^{-1}) = 0.75 \times (\log[L_{FUV}(\mathrm{W\ Hz}^{-1})] - 21.5) + 0.17 \tag{B.5}$$

Salim et al. (2007) – *GALEX*-SDSS DR3 (48 295 galaxies at $0.005 < z < 0.22$) – Chabrier IMF

$$\log(SFR_{NUV})\ (M_\odot\ \mathrm{yr}^{-1}) = \log[L_{NUV}(\mathrm{W\ Hz}^{-1})] - 21.14 \tag{B.6}$$

$$\log(SFR_{FUV})\ (M_\odot\ \mathrm{yr}^{-1}) = \log[L_{NUV}(\mathrm{W\ Hz}^{-1})] - 21.16 \tag{B.7}$$

Rosa-González et al. (2002) – 31 nearby star-forming galaxies – Salpeter IMF – Attenuation correction included

$$\log(\mathrm{SFR}_{UV})\ (M_\odot\ \mathrm{yr}^{-1}) = \log[L_{UV}(\mathrm{W\ Hz}^{-1})] - 20.19 \tag{B.8}$$

B.2. u band

Davies et al. (2016) – GAMA II survey (3749 galaxies at $z < 0.13$) – Chabrier IMF

$$\log(SFR_u)\ (M_\odot\ \mathrm{yr}^{-1}) = 0.92 \times (\log[L_u(\mathrm{W\ Hz}^{-1})] - 21.25) - 0.079 \tag{B.9}$$

Moustakas et al. (2006) – SDSS (120 846 galaxies at $z \sim 0.1$) – Salpeter IMF – Attenuation correction included

$$\log(\mathrm{SFR_u})\ (M_\odot\ \mathrm{yr}^{-1}) = \log[L_u(\mathrm{erg\ s}^{-1})]] - 42.85 \tag{B.10}$$

Figueira, Pollo, KM+2023

MOTIVATION

Determination of a galaxy's **star formation rate** (SFR) and **stellar mass**, also for LSBs, is critical for the studies of galaxy evolution.

SFR indicators proposed and utilised over the years are based on the:

- nebular line emission (i.e. Hα, Hβ, OII), and
- the stellar continuum emission

  (i.e. SED - modelling)
- SFR calibrators for star forming galaxies
- and others ...

MOTIVATION

Determination of a galaxy's **star formation rate** (SFR) and **stellar mass**, also for LSBs, is critical for the studies of galaxy evolution.

SFR indicators proposed and utilised over the years are based on the:

- nebular line emission (i.e. Hα, Hβ, OII), and
- the stellar continuum emission (i.e. SED - modelling)
- SFR calibrators for star forming galaxies
- and others ...

All methods are critically limited by our ability to correct for the effects of DUST.

This usually required IR and/or UV data.

MOTIVATION

Role of dust in galaxies:

- **DUST** is a key component in a galaxy's evolution,
- it affects the observations, especially at shorter wavelengths - known as **attenuation** - a crucial quantity to consider while estimating galaxy properties,

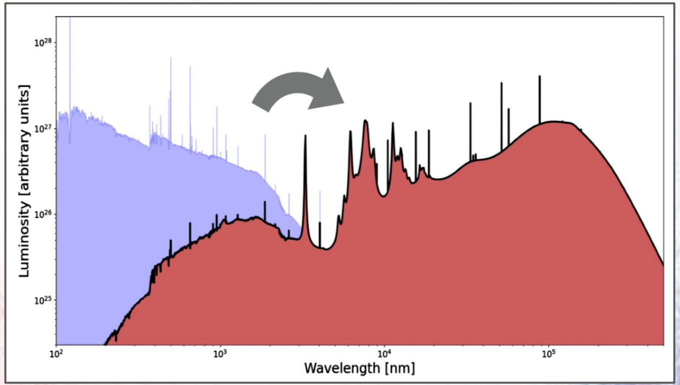

Credit: Mahmoud Hamed

MOTIVATION DUST ATTENUATION:

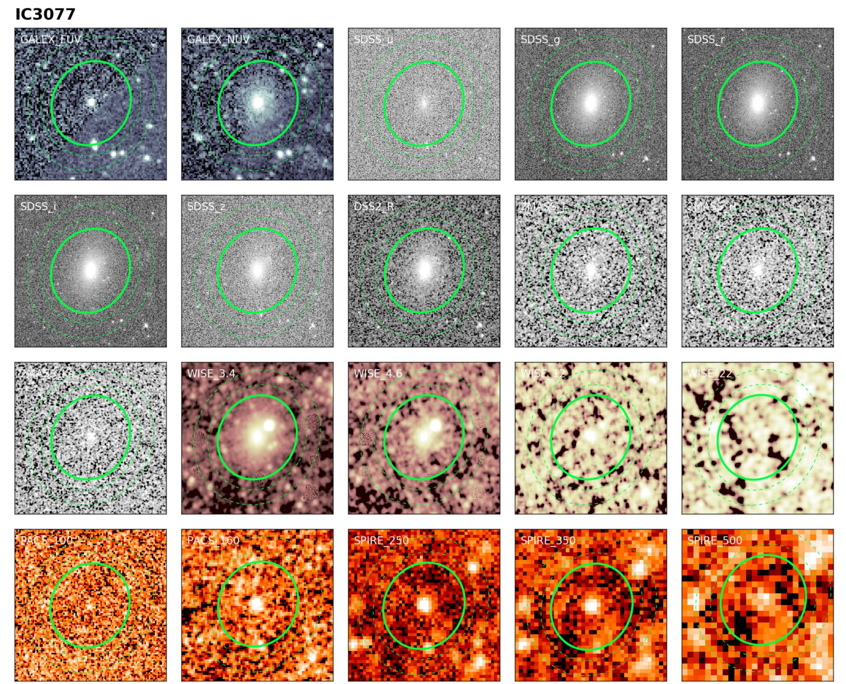

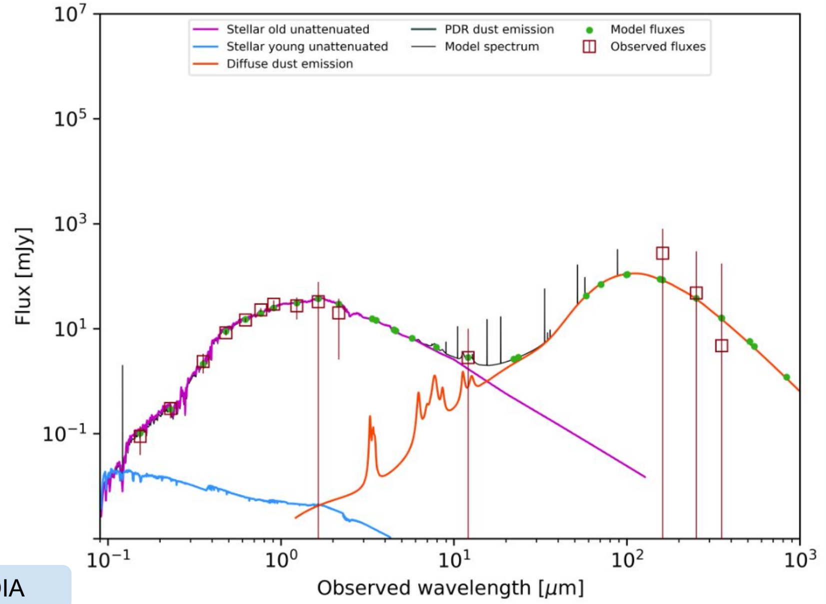

DUSTPEDIA

IC3077 (z=0.005) : SFR ($M_\odot$/yr): 0.0004±0.0002,
M_{star} ($M_\odot$): $5.06\times10^8 \pm 1.01\times10^8$, M_{dust} ($M_\odot$): $9.44\times10^3 \pm 2.1610^4$,
Att. FUV: 0.07±0.08 mag, T_{dust} (K): 28.6±0.3

MOTIVATION DUST ATTENUATION:

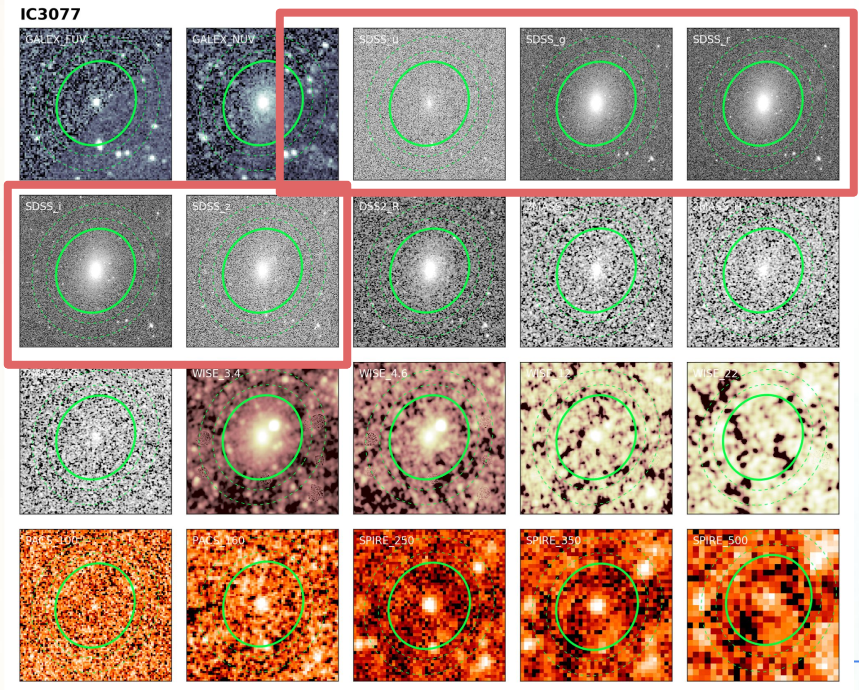

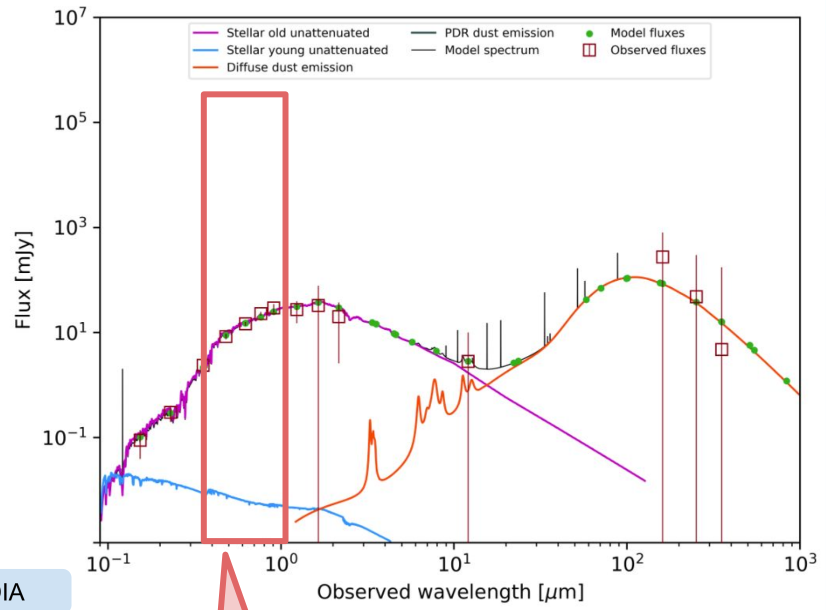

DUSTPEDIA

IC3077 (z=0.005) : SFR ($M_\odot$/yr): 0.0004±0.0002,
M_{star} ($M_\odot$): 5.06x10^8±1.01x10^8 , M_{dust} ($M_\odot$): 9.44x10^3±2.16x10^4,
Att. FUV: 0.07±0.08 mag, T_{dust} (K): 28.6±0.3

LSST

MOTIVATION DUST ATTENUATION:

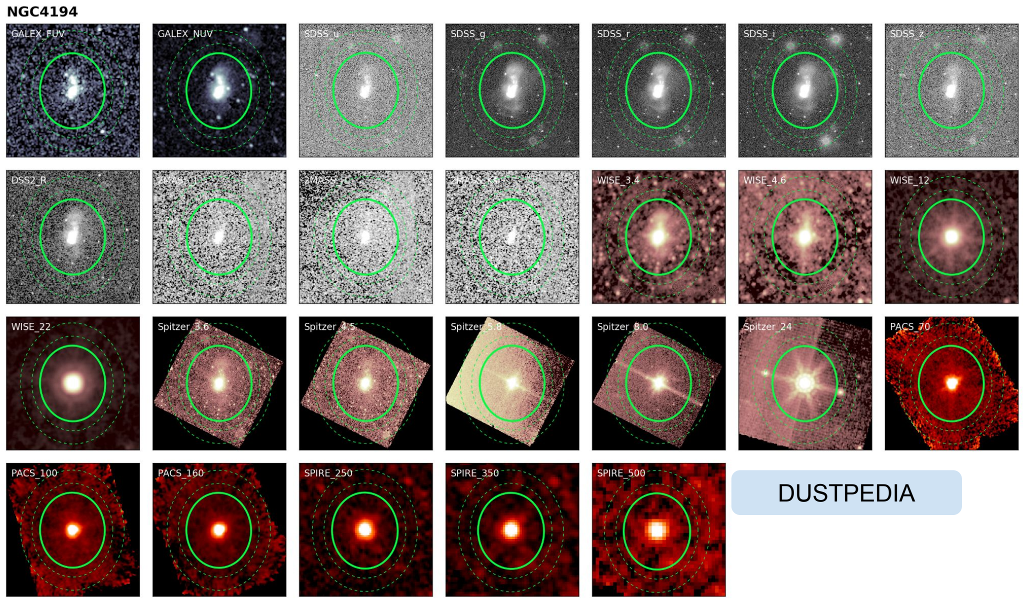

DUSTPEDIA

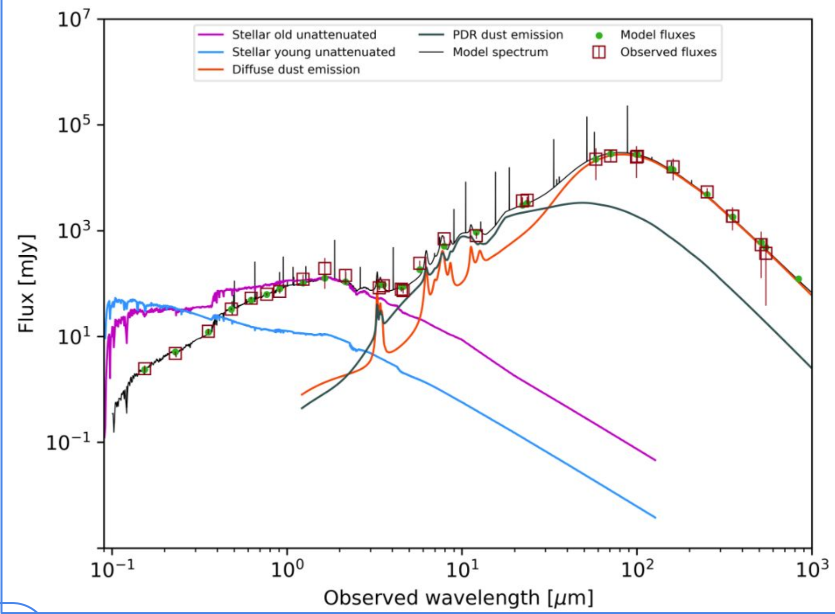

NGC4194 (z=0.008) SFR($M_\odot$/yr): 16±0.8,
M_{star}($M_\odot$): 1.3x10^{10}±3.2x10^{9} , M_{dust} ($M_\odot$): 7.25x10^{6}±3.62x10^{5}
Att. FUV: 3.8±0.2 mag; T_{dust}(K): 37.0±0.1

MOTIVATION DUST ATTENUATION:

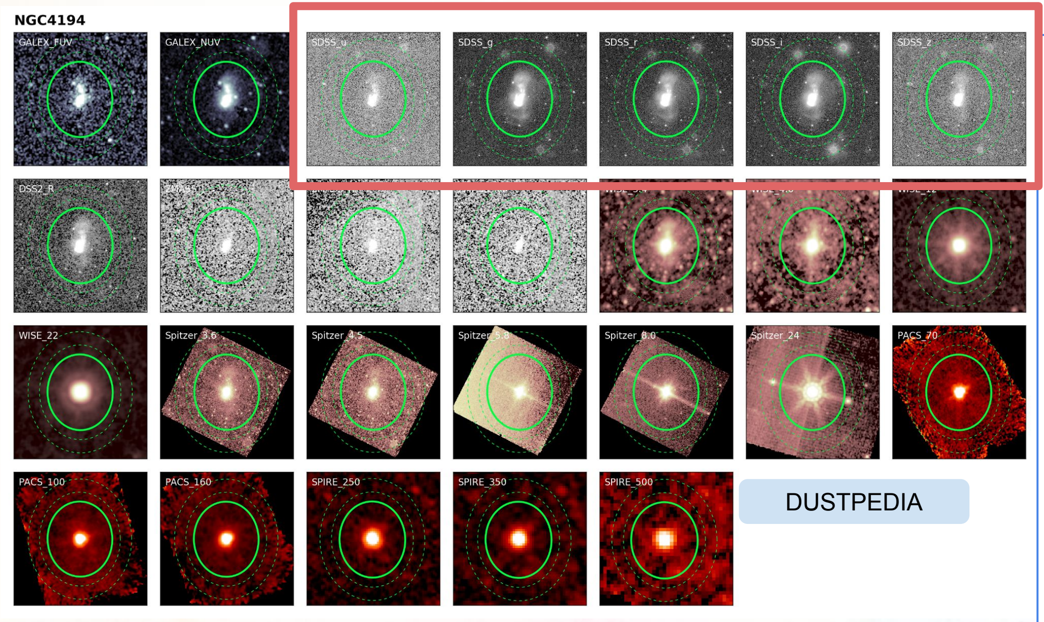

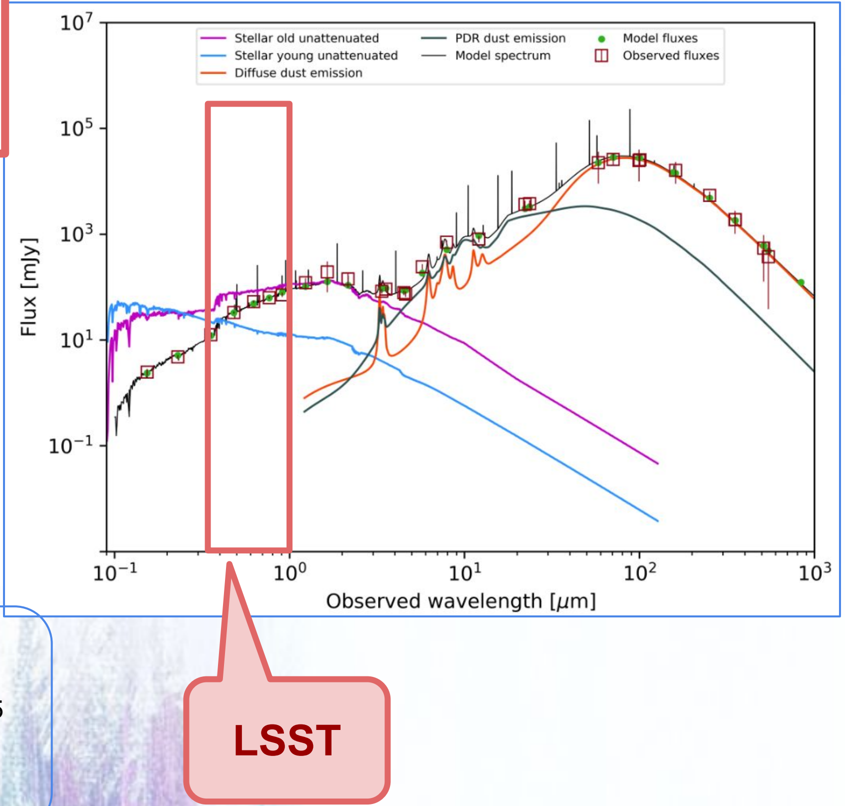

NGC4194 (z=0.008) SFR($M_\odot$/yr): 16±0.8,
M_{star}($M_\odot$): 1.3x10^{10}±3.2x10^9 , M_{dust} ($M_\odot$): 7.25x10^6±3.62x10^5
Att. FUV: 3.8±0.2 mag; T_{dust}(K): 37.0±0.1

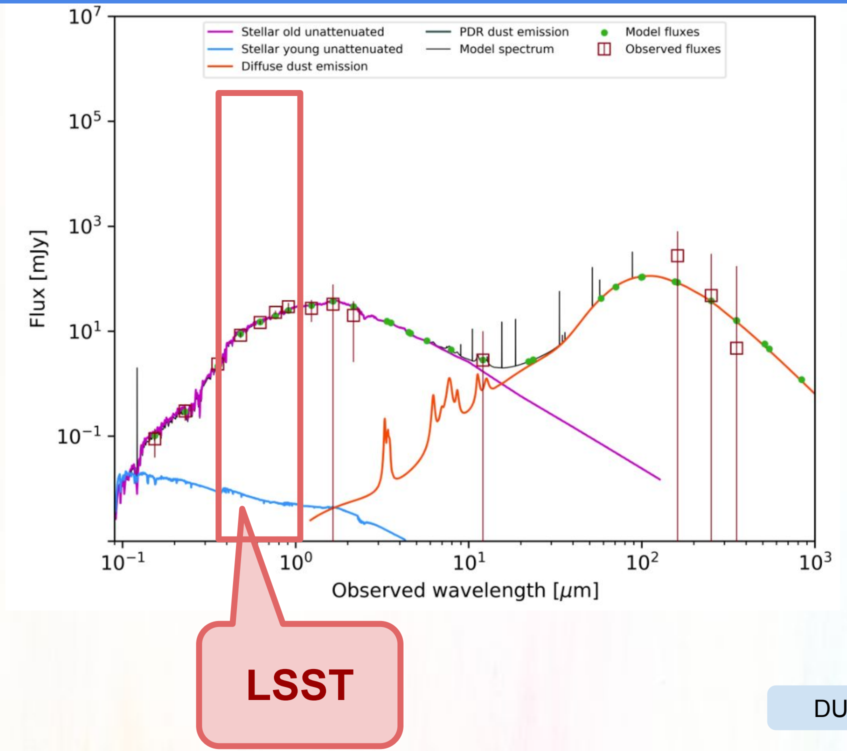

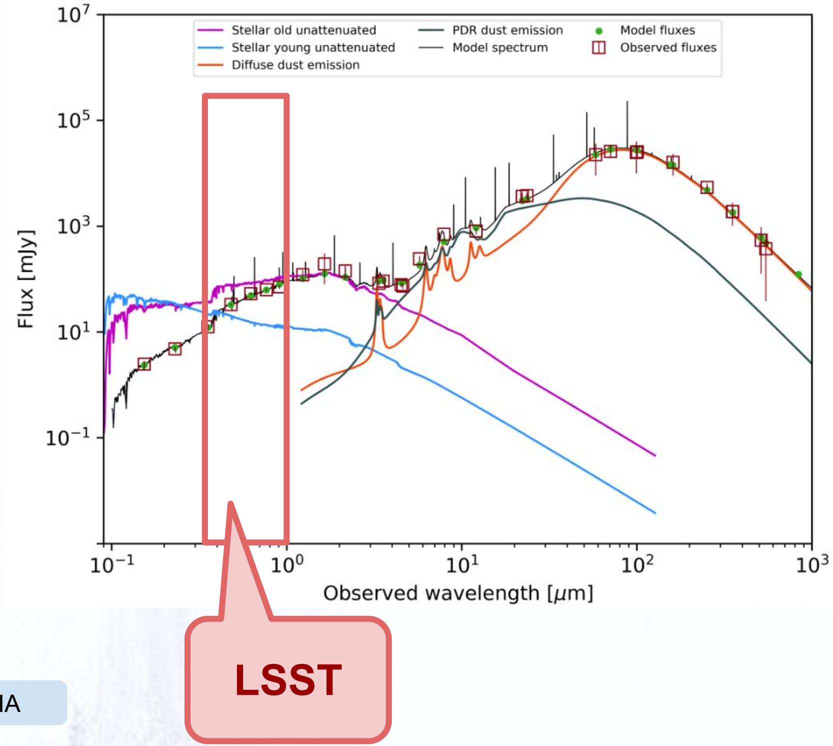

DUSTPEDIA

IC3077 (z=0.005) : SFR ($M_\odot$/yr): 0.0004±0.0002, M_{star} ($M_\odot$): $5.06\times10^8 \pm 1.01\times10^8$, M_{dust} ($M_\odot$): $9.44\times10^3 \pm 2.16\times10^4$, **Att. FUV: 0.07±0.08** mag, T_{dust} (K): 28.6±0.3

NGC4194 (z=0.008) SFR($M_\odot$/yr): 16±0.8, M_{star}($M_\odot$): $1.3\times10^{10} \pm 3.2\times10^9$, M_{dust}($M_\odot$): $7.25\times10^6 \pm 3.62\times10^5$, **Att. FUV: 3.8±0.2** mag; T_{dust}(K): 37.0±0.1

MOTIVATION

Role of attenuation in stellar mass estimation:

- Attenuation affects the stellar mass estimate: Calzetti+2000 law (single power law) gives **lower** stellar masses than Charlot & Fall 2000 (two components: birth cloud + ISM): KM+2018, Buat+2019, Hamed, KM+2023

ELAIS N1 ~50k observed galaxies

similar results: Buat+2019, Hamed+2023

Małek+2018

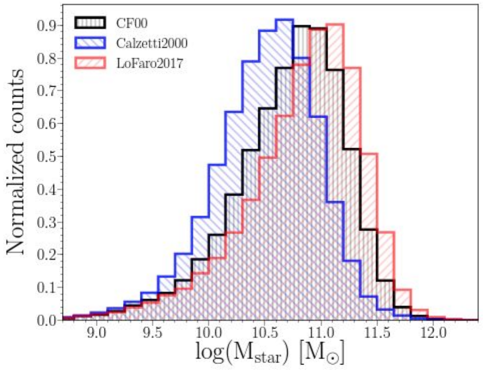

Fig. 8. Comparison of stellar masses obtained with three different dust attenuation laws: Charlot & Fall (2000) – black striped histogram, Calzetti et al. (2000) – blue right hatched histogram, and Lo Faro et al. (2017) – red left hatched histogram.

MOTIVATION

Role of attenuation in stellar mass estimation:

- Attenuation affects the stellar mass estimate: Calzetti+2000 law (single power law) gives **lower** stellar masses than Charlot & Fall 2000 (two components: birth cloud + ISM): KM+2018, Buat+2019, Hamed, KM+2023
- the relative geometrical extent of the emission coming from the stellar and the dust regions, is crucial in determining the dust right attenuation curve.

Buat+2019

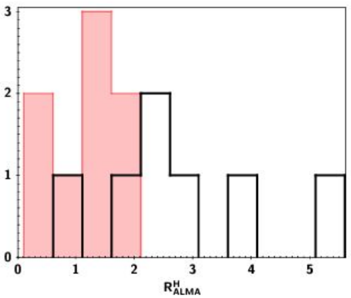

Fig. 13. Histogram of the ratio of the *H*-band radius to the ALMA radius, $R^{H}_{\rm ALMA}$. The filled histogram represents galaxies for which C00 gives a satisfying fit, and the empty histogram represents galaxies for which a shallower power-law attenuation (CF00 or LF17) is needed.

Hamed, KM+2023

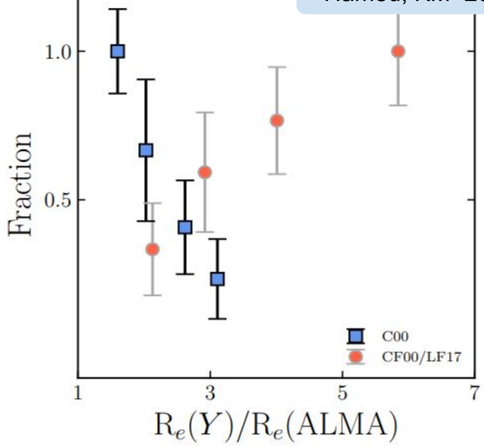

Fig. 12. Preference of attenuation laws of our sample according to the star-to-dust compactness. To facilitate the reading of this plot, we shifted the bins of CF00/LF17 slightly to the right (+0.1).

PREVIOUS WORKS

z=0.92

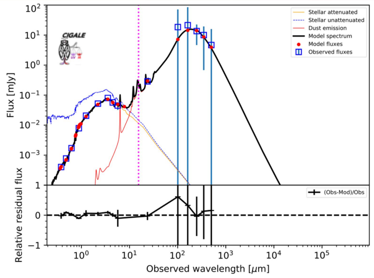

Real data from the ELAIS N1 same. Full UV-to-IR observations fitted using CIGALE software. The blue square represents the observed fluxes, and red dots represent the fluxes predicted by the model.

M_{star}=6.05x10^{10} +/- 5.62x10^{9} M_{sun},
SFR=11.90+/-2.16 M_{sun}/yr

Riccio, KM et al. 2021

PREVIOUS WORKS

z=0.92

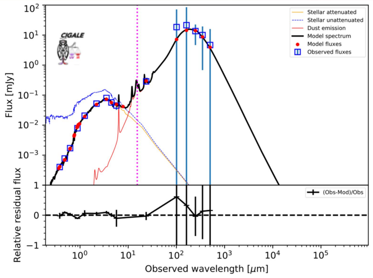

Real data from the ELAIS N1 same. Full UV-to-IR observations fitted using CIGALE software. The blue square represents the observed fluxes, and red dots represent the fluxes predicted by the model.

M_{star}=6.05x10^{10} +/- 5.62x10^{9} M_{sun},
SFR=11.90+/-2.16 M_{sun}/yr

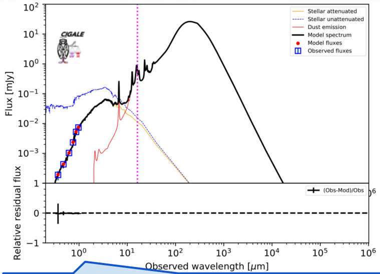

Simulated LSST observation in the six LSST bands (ugrizy; the filter response curve is provided by the Ivezić et al. 2019) based on the best model from the real galaxy

M_{star}=5.59x10^{10} +/- 1.80x10^{10} M_{sun},
SFR=67.40+/-45.90 M_{sun}/yr

Riccio, KM et al. 2021

PREVIOUS WORKS

z=0.92

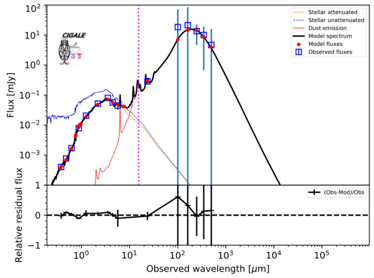

Real data from the ELAIS N1 same. Full UV-to-IR observations fitted using CIGALE software. The blue square represents the observed fluxes, and red dots represent the fluxes predicted by the model.

M_{star}=6.05x10^{10} +/- 5.62x10^{9} M_{sun},
SFR=11.90+/-2.16 M_{sun}/yr

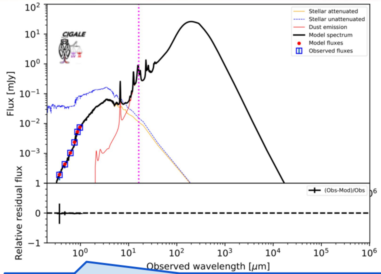

Simulated LSST observation in the six LSST bands (ugrizy; the filter response curve is provided by the Ivezić et al. 2019) based on the best model from the real galaxy

M_{star}=5.59x10^{10} +/- 1.80x10^{10} M_{sun},
SFR=67.40+/-45.90 M_{sun}/yr

Riccio, KM et al. 2021

PREVIOUS WORKS

z=0.92

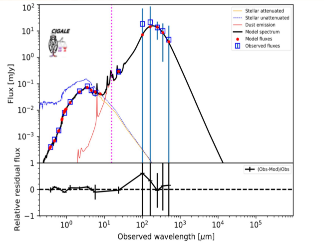

M_{star}=6.05x10^{10} +/- 5.62x10^{9} M_{sun},
SFR=11.90+/-2.16 M_{sun}/yr

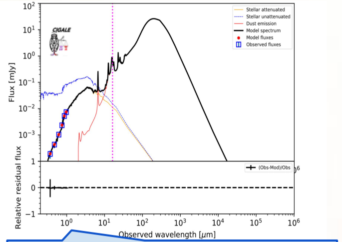

M_{star}=5.59x10^{10} +/- 1.80x10^{10} M_{sun},
SFR=67.40+/-45.90 M_{sun}/yr

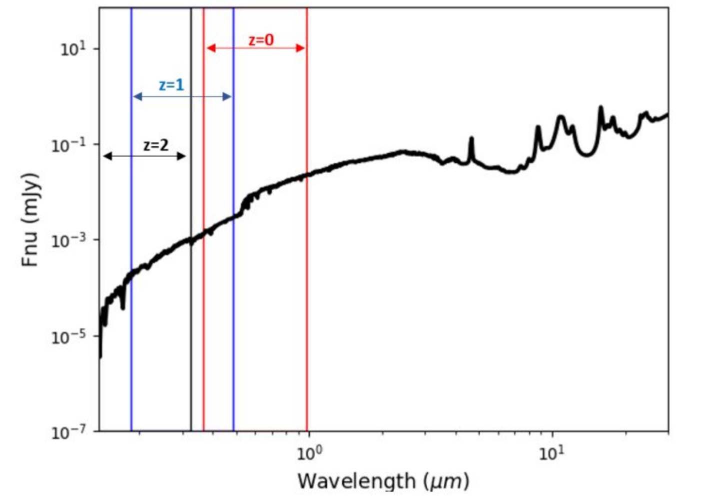

Fig. 8. LSST coverage of an example SED at different redshifts indicated in the panel.

Riccio, KM et al. 2021

At redshift ~0 LSST probes mainly old stellar population, without any band probing young stellar population or dust properties. As redshift increases, the LSST ugriz filters start to cover the UV rest frame, and the estimates of the SFR significantly improve.

PREVIOUS WORKS

z=0.92

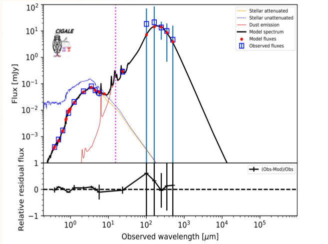

M_{star}=6.05x10^{10} +/- 5.62x10^{9} M_{sun},
SFR=11.90+/-2.16 M_{sun}/yr

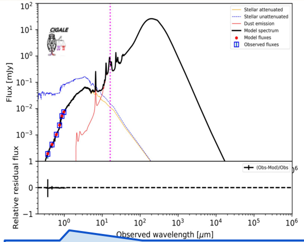

M_{star}=5.59x10^{10} +/- 1.80x10^{10} M_{sun},
SFR=67.40+/-45.90 M_{sun}/yr

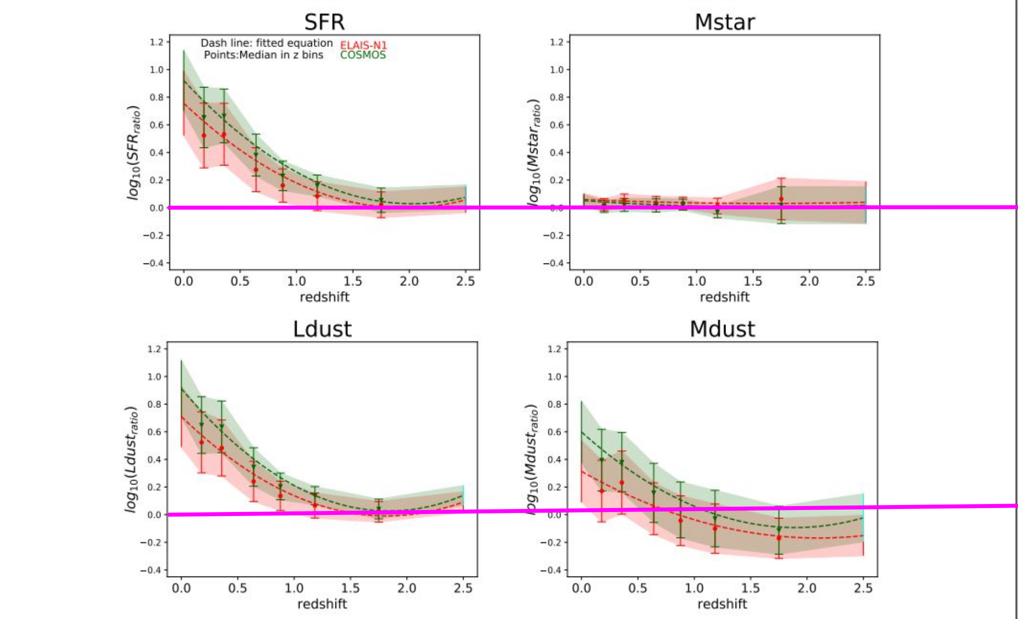

Fig. 7. Ratios of different physical properties obtained from fitting the simulated LSST data alone and from the UV-FIR SED (e.g., $SFR_{ratio} = SFR_{LSST}/SFR_{UV-FIR}$) as a function of redshift for the ELAIS N1 and COSMOS fields. The properties obtained from the UV-FIR SED fitting are considered as the true values. *From the upper left panel* we show clockwise the SFR, M_{star}, L_{dust}, and M_{star} comparisons. The dashed lines represent polynomial fits performed on the samples. The points are the median values in each redshift bin, with the median absolute deviation as errors. A ratio equal to zero corresponds to a perfect agreement between the estimates obtained based on the LSST-like sample and the real values. The distributions calculated for ELAIS N1 and COSMOS are comparable within the errors.

everything-is-fine line

Riccio, KM et al. 2021

PREVIOUS WORKS

In Riccio+21 we calculated A_{FUV} proxy thanks to the multi-λ data of ELAIS N1 & COSMOS field.

$$A_{\mathrm{FUV-LSST}} = a \cdot \log_{10}(M_{\mathrm{star-LSST}}) + b.$$

Redshift	a	b
0–0.5	0.41 ± 0.02	-1.39 ± 0.21
0.5–1	0.44 ± 0.03	-0.49 ± 0.30
1–1.5	0.72 ± 0.03	-3.42 ± 0.34
1.5–2.5	0.83 ± 0.04	-5.19 ± 0.39

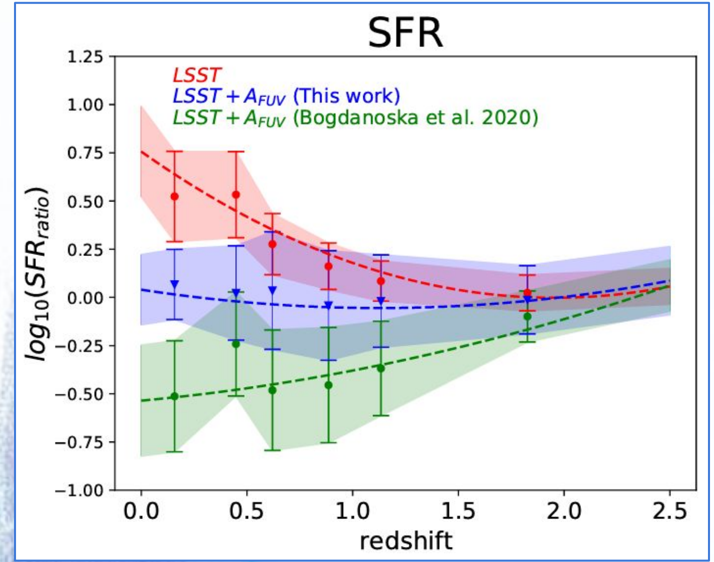

In Riccio+21 we calculated A_{FUV} proxy thanks to the multi-λ data of ELAIS N1 & COSMOS field.

Can we use LSST-like data (fluxes, colours, morphological parameters) to proxy AFUV without having to rely on other surveys?

We did our best to try it.

Małek, Junais, Pollo et al., 2024

Selection criteria	Number of selected sources	% of the initial sample
catalogue of physical properties (Salim et al. 2016, 2018)		
GSWLC-X2	659 229	100,0%
objects with A_{FUV} estimation	650 597	98.7%
Main Galaxy Survey flag_msg=1	610 518	92.6%
SED fitting flag=0 (all SDSS photometry, no broad-line spectrum)	603 615	91.6%
at least one GALEX detection (FUV or NUV)	404 830	61.4%
medium and deep UV exposure time (GSWLC-A and D)	252 445	38.3%
L_{TIR} estimated based on the WISE 22μm	82 116	12.6%
REDCHISQ<5 (goodness of the fit, following Salim et al. 2016, 2018)	78 725	11.9%
photometric catalogue Alam et al. (2015)		
cross-matching with SDSS Alam et al. (2015) catalogue	78 725	11.9%
cleaning based on the SDSS flags (Sec. 3.2)	44 047	6.7%
morphological catalogue Meert et al. (2015)		
cross-matching with Meert et al. (2015) catalogue	29 593	4.5%
the axis ratio of the total fit > 0	29 487	4.5%
Selection based on Sec. 3.4:		
redshift range 0.025–0.1	9 596	1.5%
main sequance galaxies	7 934	1.2%

Physical properties

Photometric data

morphological data

Redshift & main sequence selection

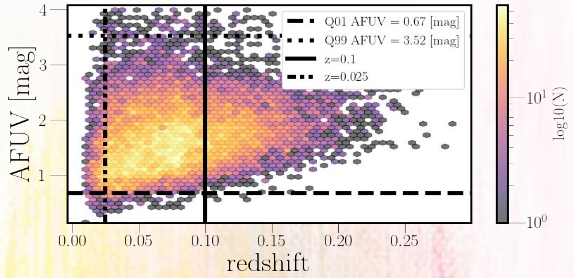

Why redshift and A_{FUV} cuts?

Małek, Junais, Pollo +2024

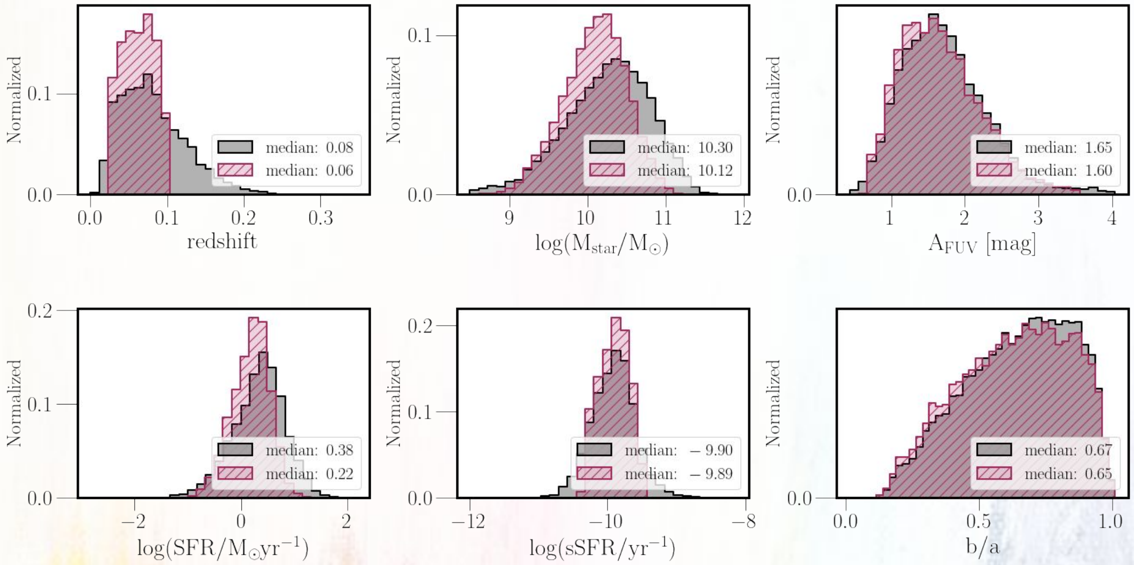

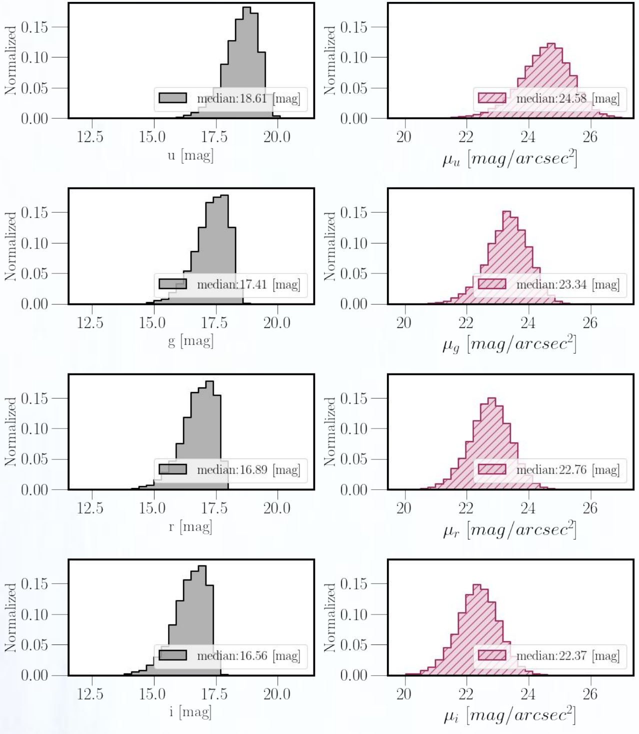

Surface brightness corrected for inclination and redshift

Małek, Junais, Pollo +2024

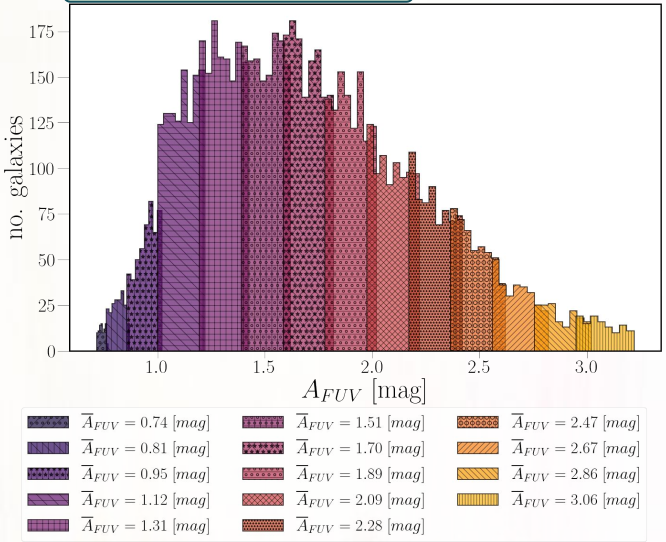

A_{FUV} bin	bin width	$\overline{A}_{FUV}$	# gal.	% sample
0.72 – 0.77	0.06	0.74	79	1.01
0.76 – 0.87	0.11	0.81	174	2.23
0.86 – 1.02	0.16	0.95	453	5.81
1.00 – 1.22	0.22	1.12	1053	13.51
1.20 – 1.42	0.23	1.31	1275	16.35
1.39 – 1.62	0.23	1.51	1277	16.38
1.59 – 1.82	0.24	1.70	1260	16.16
1.78 – 2.02	0.24	1.89	1074	13.77
1.98 – 2.22	0.25	2.09	810	10.39
2.17 – 2.42	0.25	2.28	654	8.39
2.37 – 2.62	0.25	2.47	470	6.03
2.56 – 2.82	0.26	2.67	266	3.41
2.76 – 3.02	0.27	2.86	161	2.06
2.95 – 3.22	0.27	3.06	117	1.50

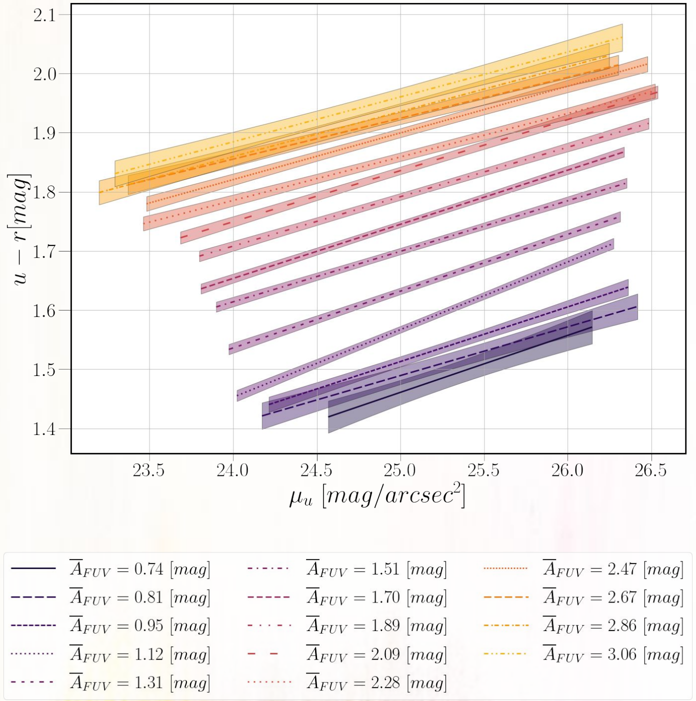

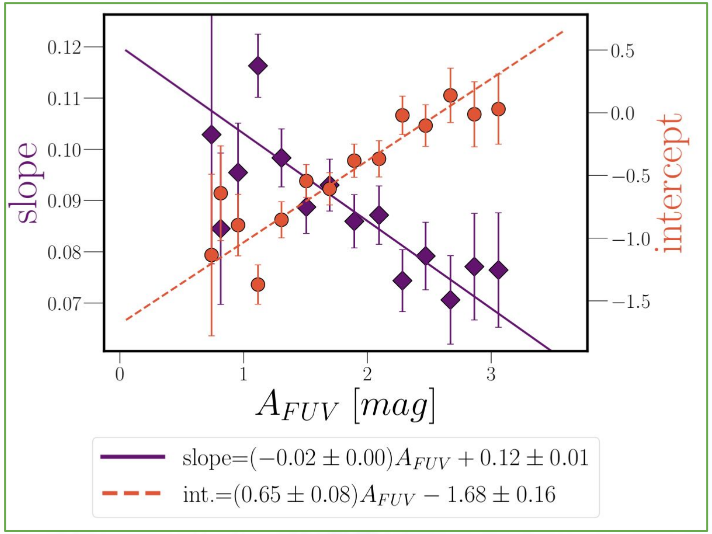

Małek, Junais, Pollo +2024

$$A_{FUVp} = \frac{(u - r) - (0.12 \cdot \mu_u) + 1.68}{(-0.02 \cdot \mu_u) + 0.65}$$

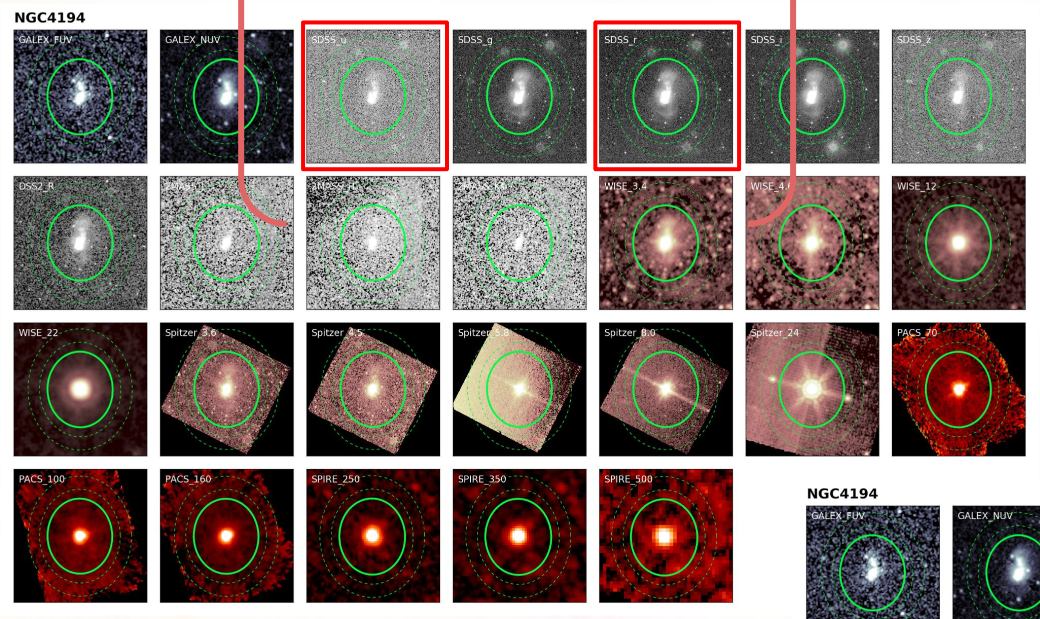
NGC4194
GALEX_FUV
GALEX_NUV
SDSS_u
SDSS_g
SDSS_r
SDSS_i
SDSS_z
DSS2_R
WISE_3.4
WISE_12
WISE_22
Spitzer_3.6
Spitzer_4.5
Spitzer_8.0
Spitzer_24
PACS_70
PACS_100
PACS_160
SPIRE_250
SPIRE_350
SPIRE_500

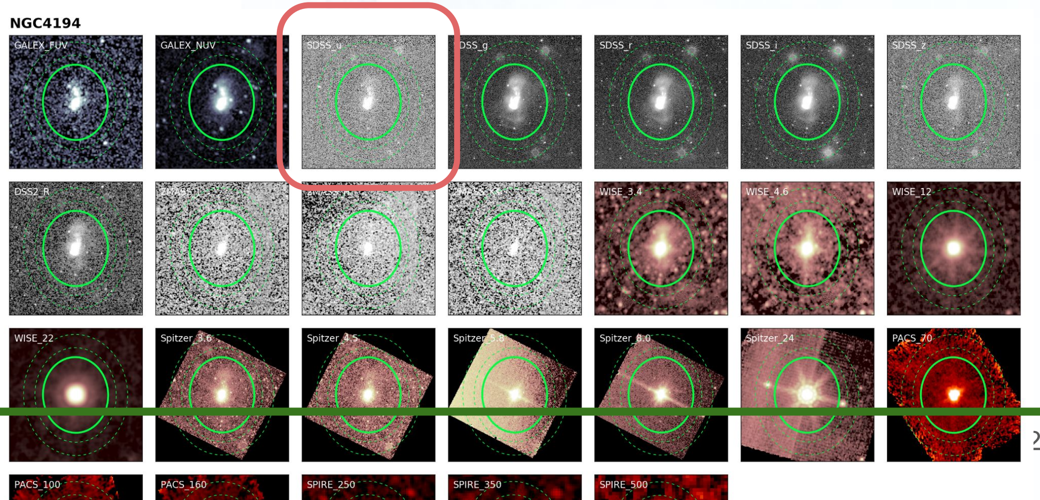
NGC4194
GALEX_FUV
GALEX_NUV
SDSS_u
SDSS_r
SDSS_i
SDSS_z
DSS2_R
WISE_3.4
WISE_4.6
WISE_12
WISE_22
Spitzer_3.6
Spitzer_4.5
Spitzer_8.0
Spitzer_24
PACS_70
PACS_100
PACS_160
SPIRE_250
SPIRE_350
SPIRE_500

DUSTPEDIA

Małek, Junais, Pollo +2024

No prior

Purely optical A_{FUV} prior

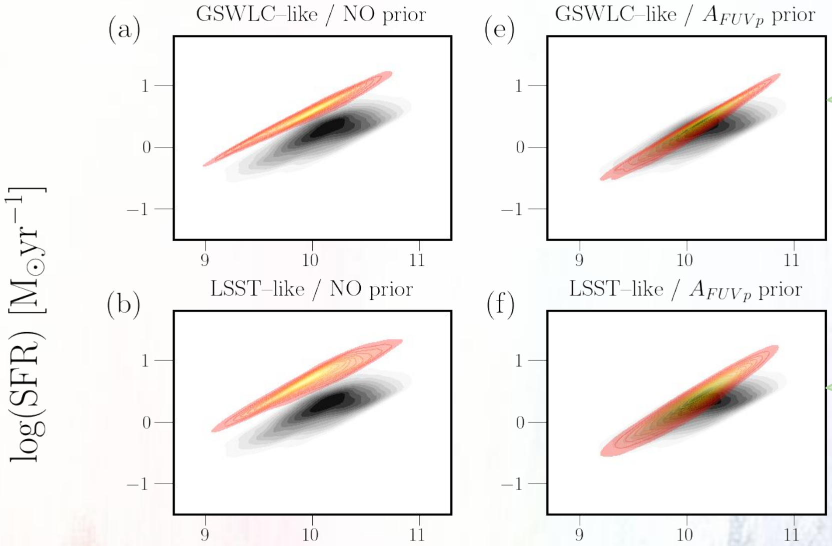

As Salim et al.,2016,2018 332 640 templates per redshift bin (203 s.)

Much smaller parameter space 5 540 templates per redshift bin (85 s.)

Computation with CIGALE SED fitting tool, Intel Core i9, 62,7 GB, 16 cores

FURTHER INVESTIGATIONS

How we can statistically check this relation for lower surface brightness regime and/or higher redshift?

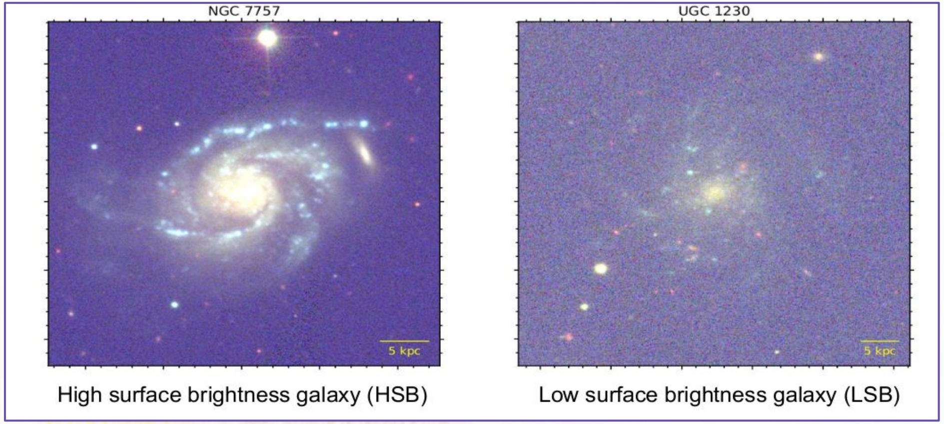

McGaugh 2021

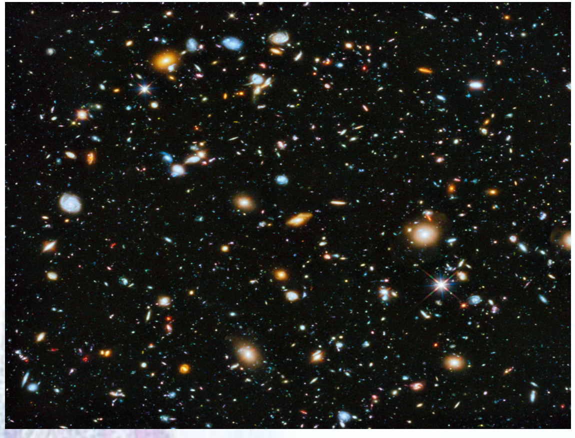

NASA, ESA, R. Ellis (Caltech), and the HUDF 2012 The Hubble Ultra Deep Field 2012

One (maybe the only?) possibility is to involve simulations.

Pushing the limits with SIMBA cosmological simulation

SIMBA is the cutting edge hydrodynamical cosmological simulation with 100 Mpc/h box size. Due to its careful dust treatment with a rich chemical evolution of the ISM, it is perfectly suited for this project.

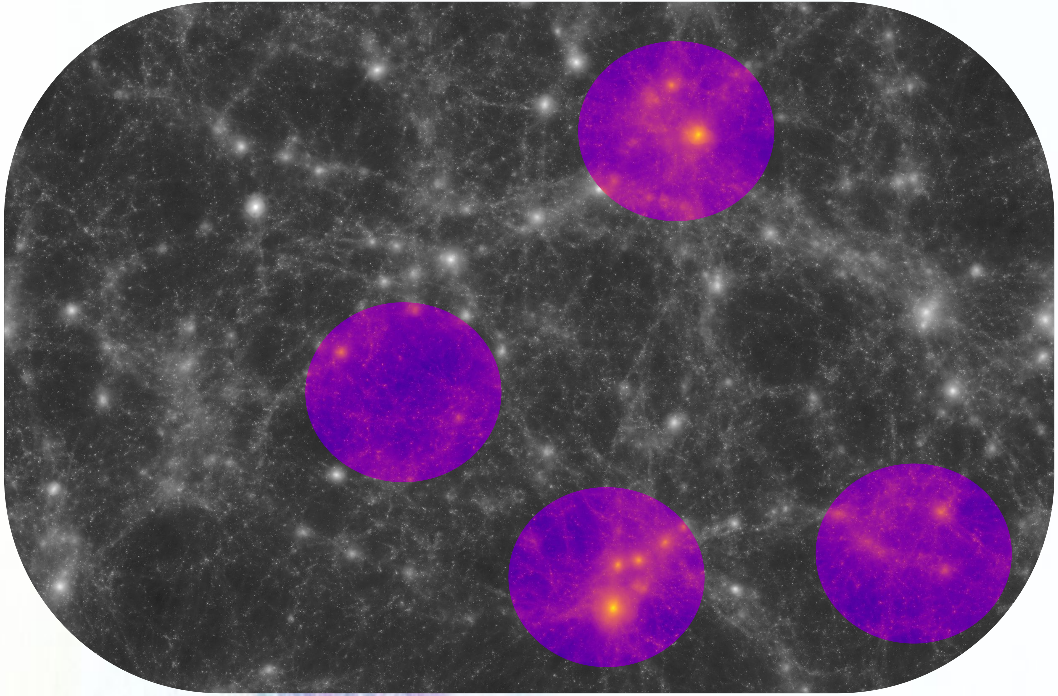

FURTHER INVESTIGATIONS

SIMBA sample selection

We calculated A_{FUV}, surface brightness, colors, etc. using SIMBA catalogs.

We tried to define the SIMBA sample as close to SDSS as possible.

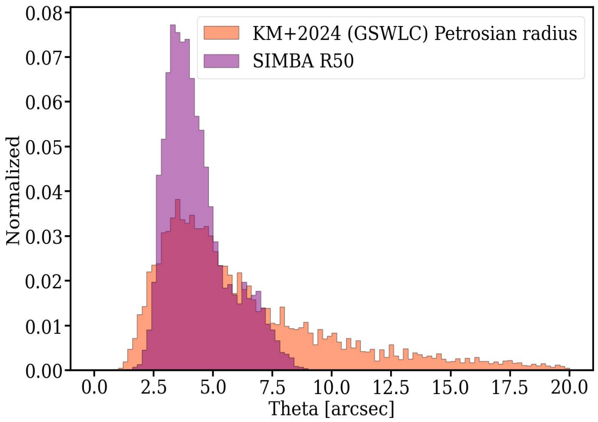

Surface brightness from Małek et al.

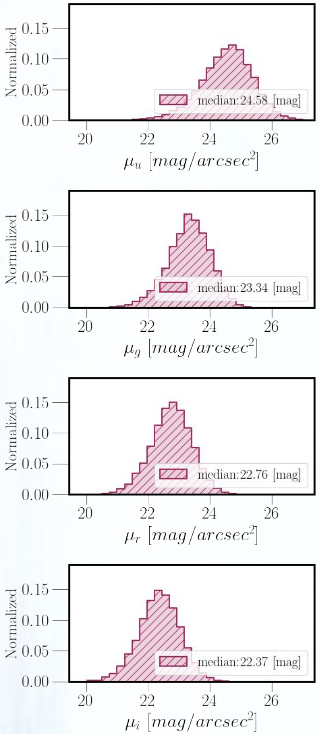

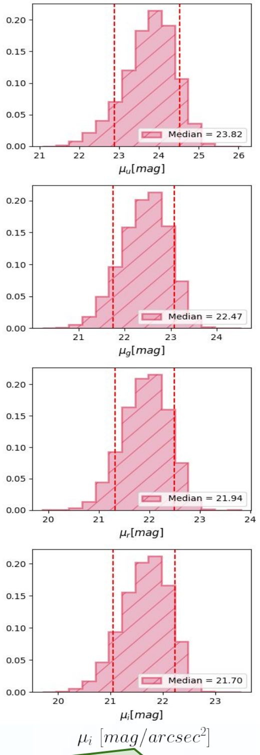

Surface brightness from SIMBA galaxies

Selection cryteria	Number of selected sources	% of the initial sample
All galaxies at z < 0.1	163431	100,00
Distance to main sequence	100471	61,48
0.67 < A_fuv < 3.71	42298	25,88
9.5 < log(M_star) < 11	17817	10,90
-10.34 < log(sSFR) < -9.49	15292	9,36
Matching u,g,r,i and z	12139	7,43
galex_nuv > 20	7508	4,59

FURTHER INVESTIGATIONS

Early results

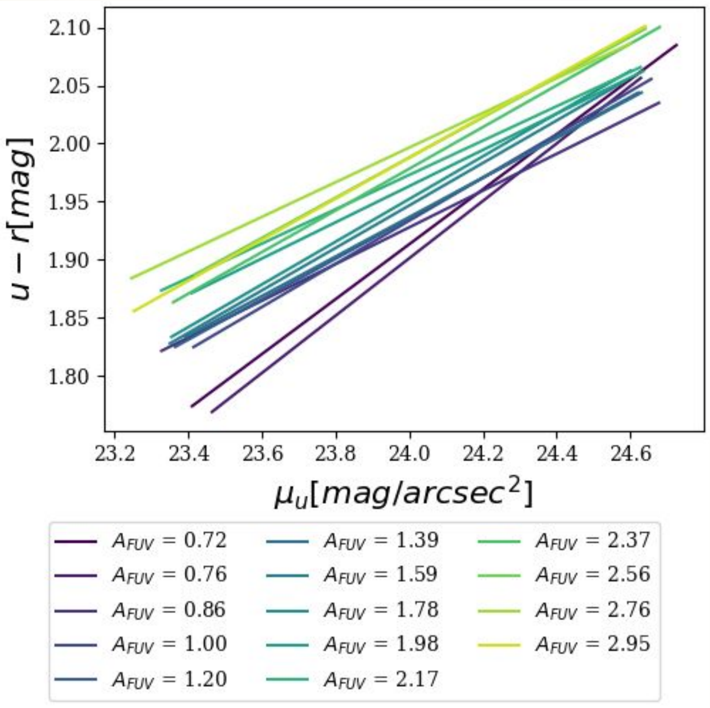

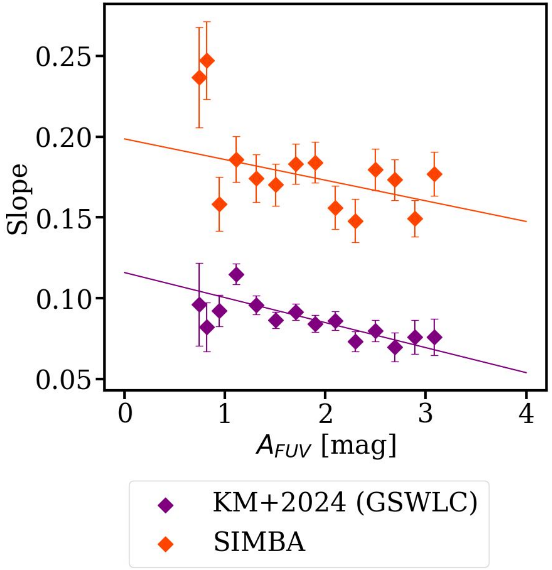

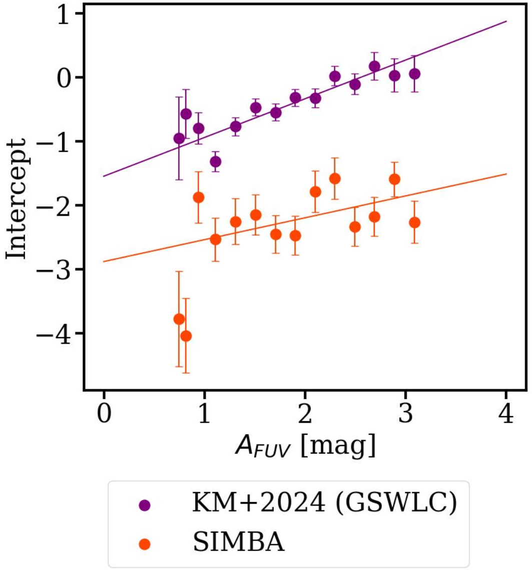

$$A_{FUV_p} = \frac{(u-r) - (0.2 \times \mu_u) + 2.87}{(-0.015 - \mu_u) + 0.4}$$

FURTHER INVESTIGATIONS

Early results

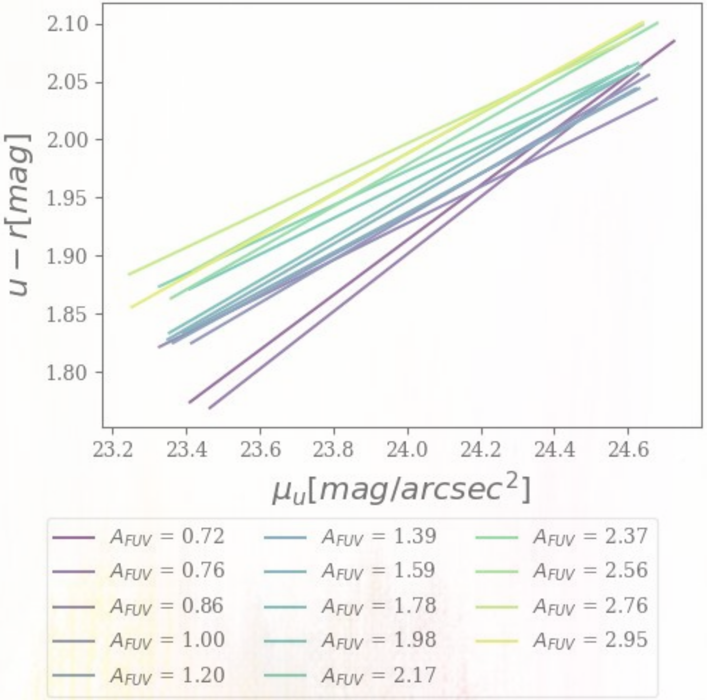

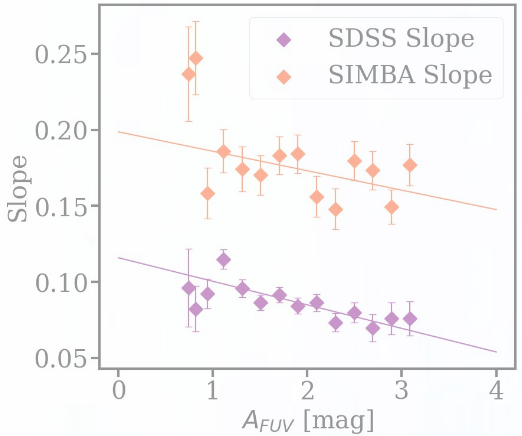

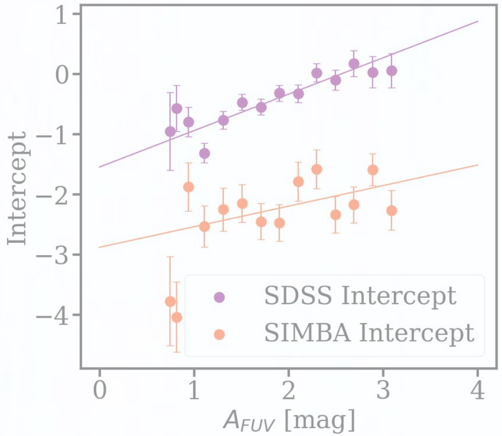

$$A_{FUVp} = \frac{(u - r) - (0.12 \cdot \mu_u) + 1.68}{(-0.02 \cdot \mu_u) + 0.65}$$

$$A_{FUV_p} = \frac{(u - r) - (0.2 \times \mu_u) + 2.87}{(-0.015 - \mu_u) + 0.4}$$

FURTHER INVESTIGATIONS

Next stages:

1) fine - tuning of obtained relations - to check if SIMBA can mimic observational data
   a) checking all possible observational cuts we had in the data used in KM et al., 2024,
   b) adding observational effects (flux blurring, observational errors, etc)
2) generalisation of the relation to galaxies of different types, not only the main sequence, and extending the analysis to lower surface brightness galaxies

We will soon contact our previous co-authors willing to expand our results. New collaborators are also welcome!

CONCLUSIONS

We have found that:

- LSST-like data needs a prior to calculate SFR,
- the best proxy for A_{FUV} can be constructed based on u-r and μ_u ,
- our A_{FUV} prior used as a proxy for the SED fitting, allows for very good recovery of SFR with only a small bias ΔSFR~0.1,
- thanks to the reduction of the number of generated templates by ~98%, we decrease the computing time needed for fitting by a comparable factor, which will be of great importance for the 'big data' analysis of the LSST data.

Thank to simulations like SIMBA we can move forward to check this relation for different types of galaxies, redshift, surface brightness etc.

Thank you for your attention

Thank you for your attention

Soon (~one/two months) we will open a call for a postdoc in the field of **BigData in the LSST era: applications to the universe of low surface brightness galaxies**. You can ask questions about the position even today!

@ slack: Katarzyna (Kasia)
malek.kasia@gmail.com
katarzyna.malek@ncbj.gov.pl

Agnieszka Pollo
agnieszka.pollo@gmail.com

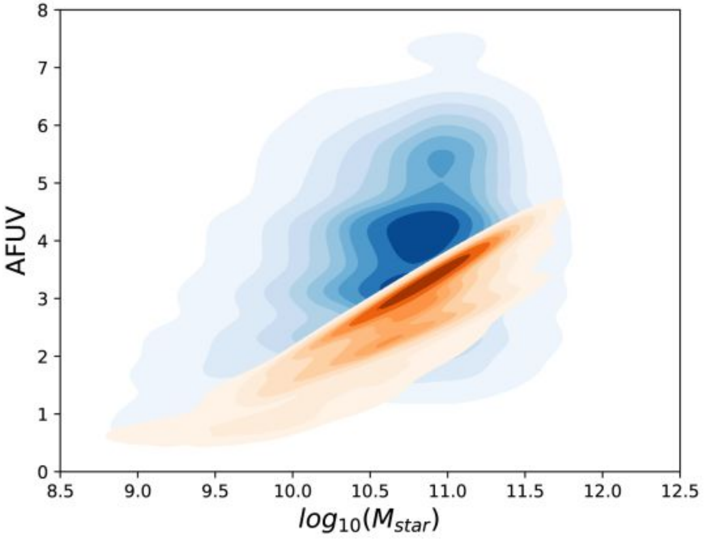

Fig. 11. $A_{\rm FUV}$ as a function of stellar mass estimated from the UV-FIR SED fitting (blue density plot) compared with the $A_{\rm FUV}$ estimated by employing $M_{\rm star}$ from the relation of Bogdanoska & Burgarella (2020).

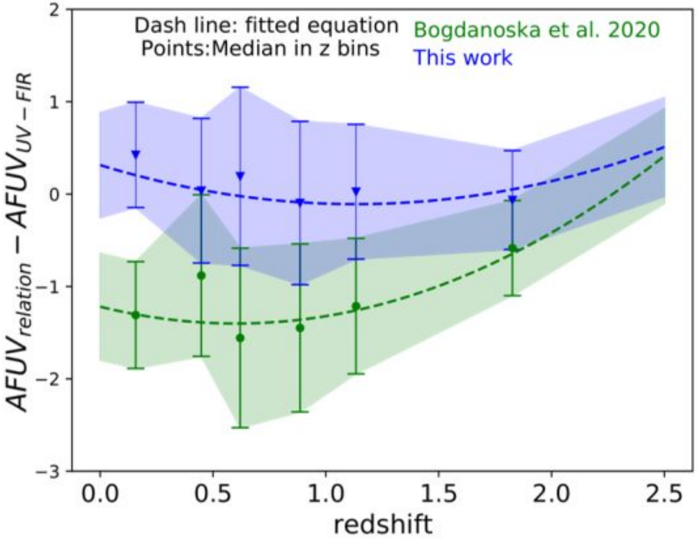

Fig. 12. Difference between $A_{\rm FUV}$ estimated from $A_{\rm FUV}$–$M_{\rm star}$ relations: Bogdanoska & Burgarella 2020 (green) and Eq. (2) with the coefficients reported in Table 5 (blue) and $A_{\rm FUV}$ estimated from the UV-FIR SED fitting as a function of redshift.

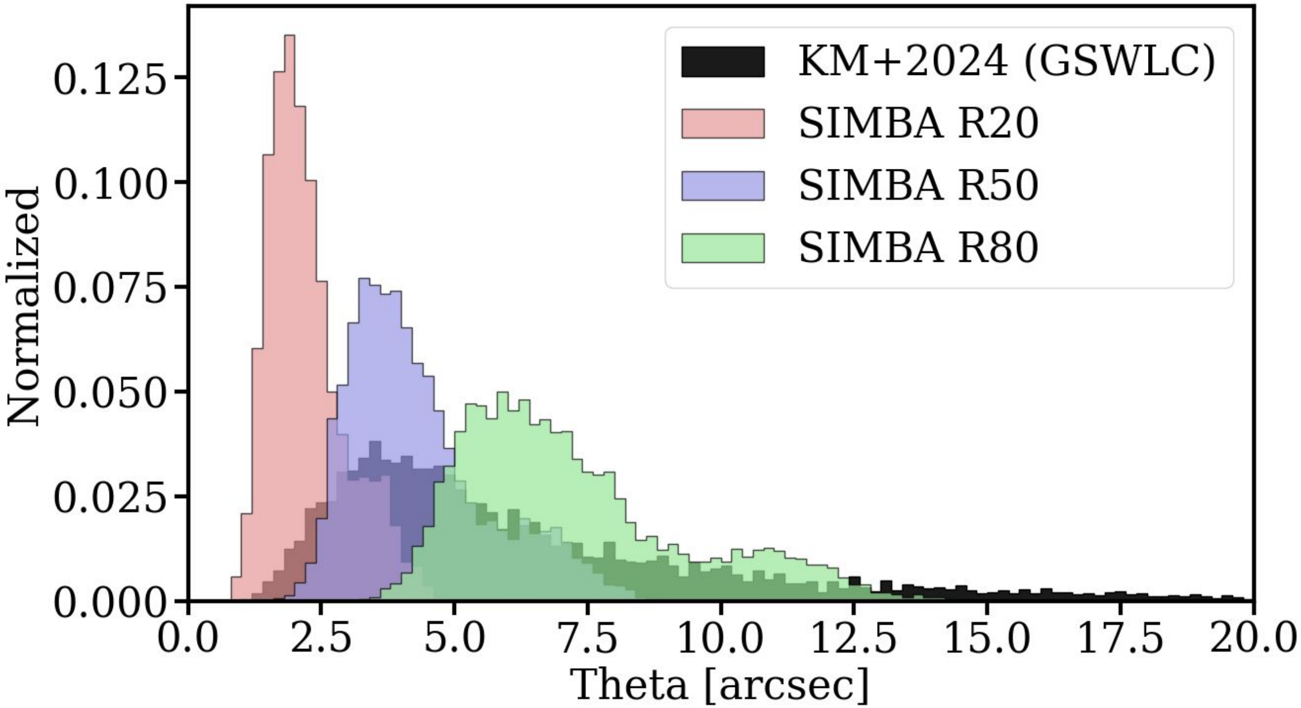
KM+2024 (GSWLC)
SIMBA R20
SIMBA R50
SIMBA R80
Normalized
0.000
0.025
0.050
0.075
0.100
0.125
0.0
2.5
5.0
7.5
10.0
12.5
15.0
17.5
20.0
Theta [arcsec]

SDSS Data Release 7
Schawinski+2014

SIMBA

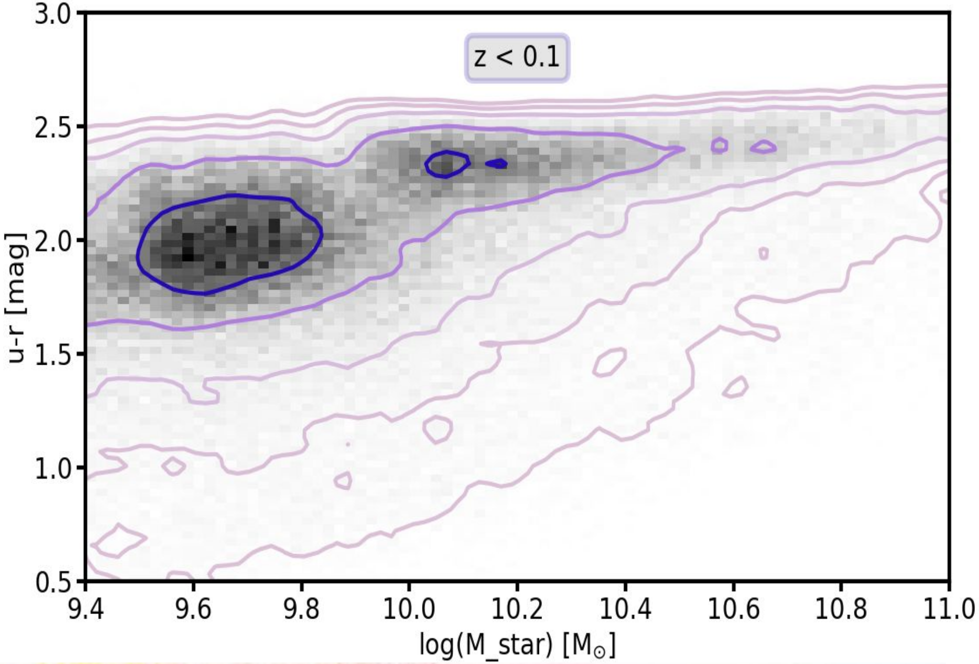

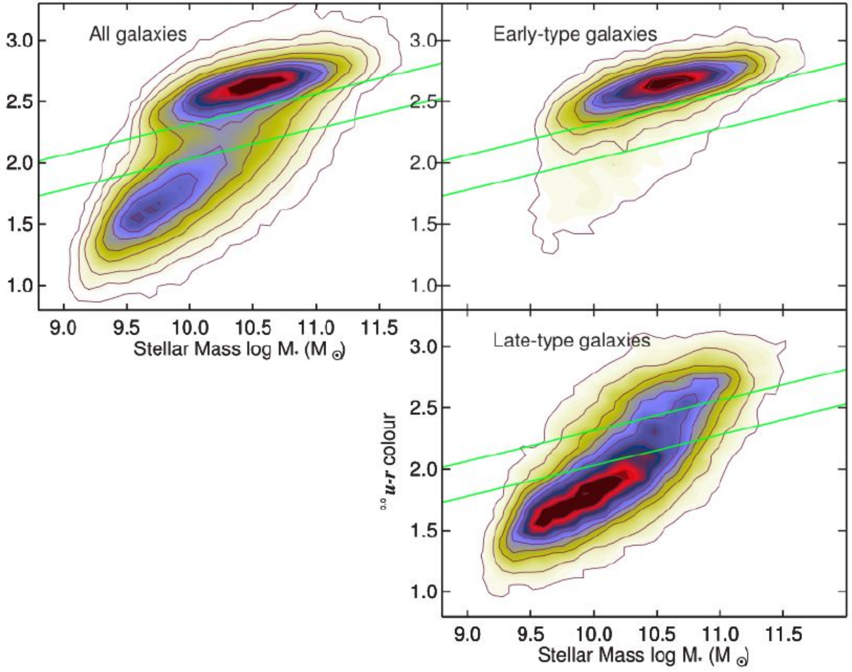

Figure 4: Color (u-r)-stellar mass diagram for all galaxies combined (top left), and for early-type and late-type galaxies separately. The green lines show the position of the green valley, which separates the red sequence above it from the blue cloud below it. Reproduced from Schawinski et al (2014).

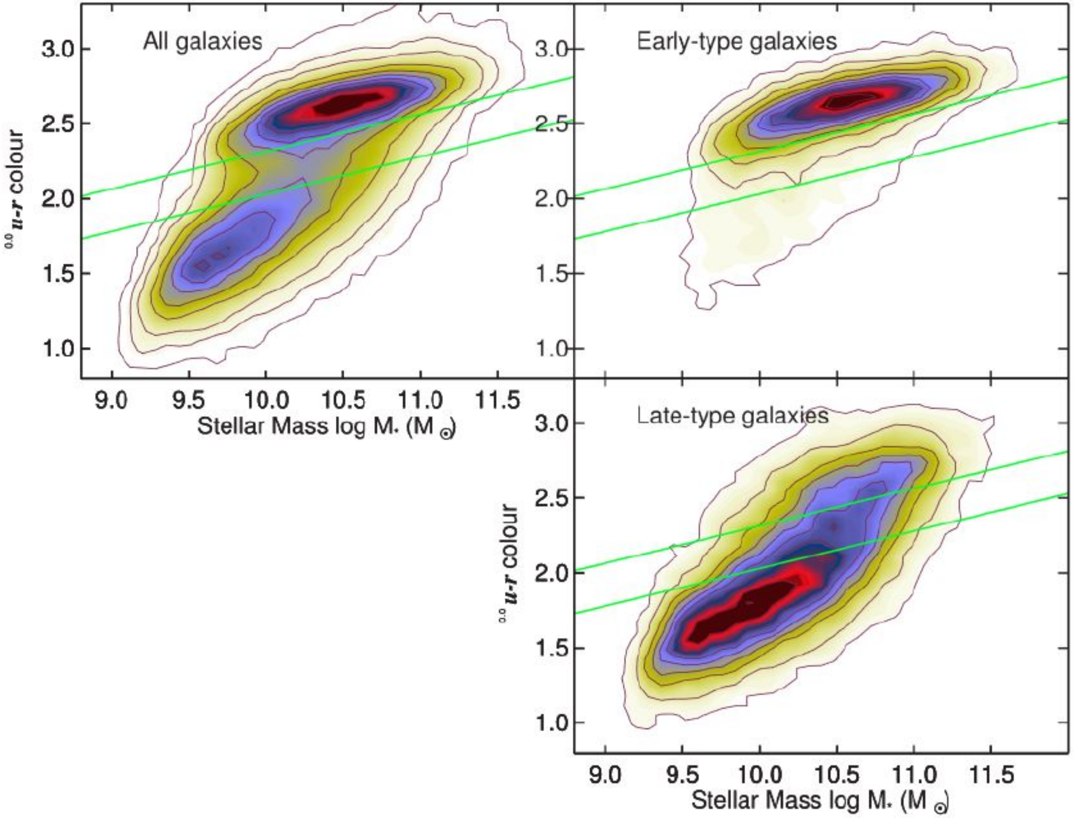

Figure 4: Color (u-r)-stellar mass diagram for all galaxies combined (top left), and for early-type and late-type galaxies separately. The green lines show the position of the green valley, which separates the red sequence above it from the blue cloud below it. Reproduced from Schawinski et al (2014).

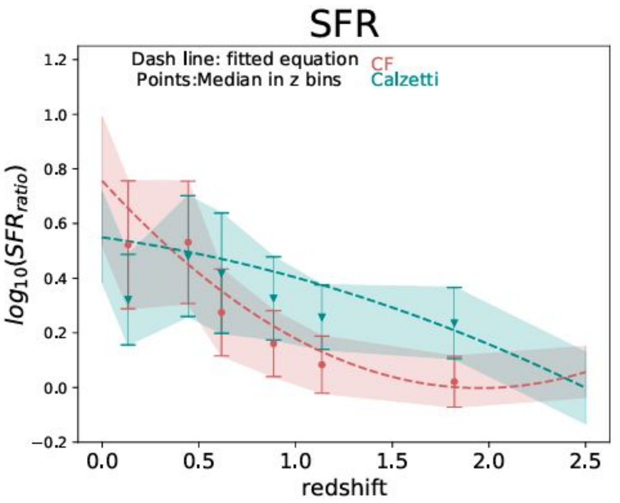

Fig. 10. SFR overestimation as a function of redshift for the Charlot & Fall (2000) (red) and Calzetti et al. (2000) (cyan) attenuation laws.

Małek, Junais, Pollo +2024

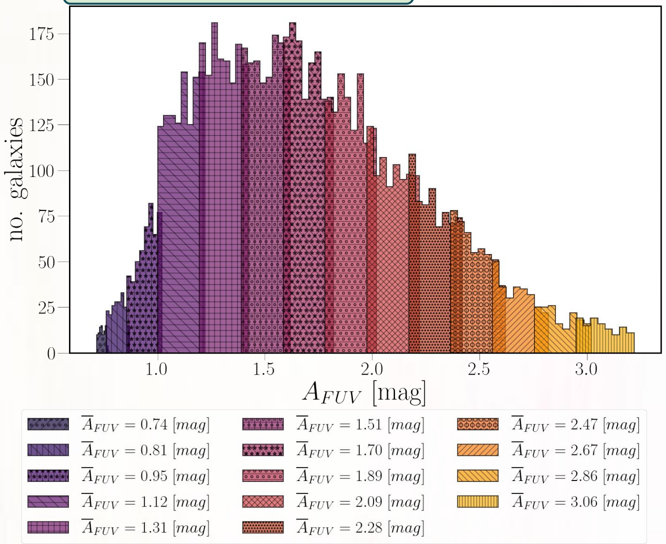

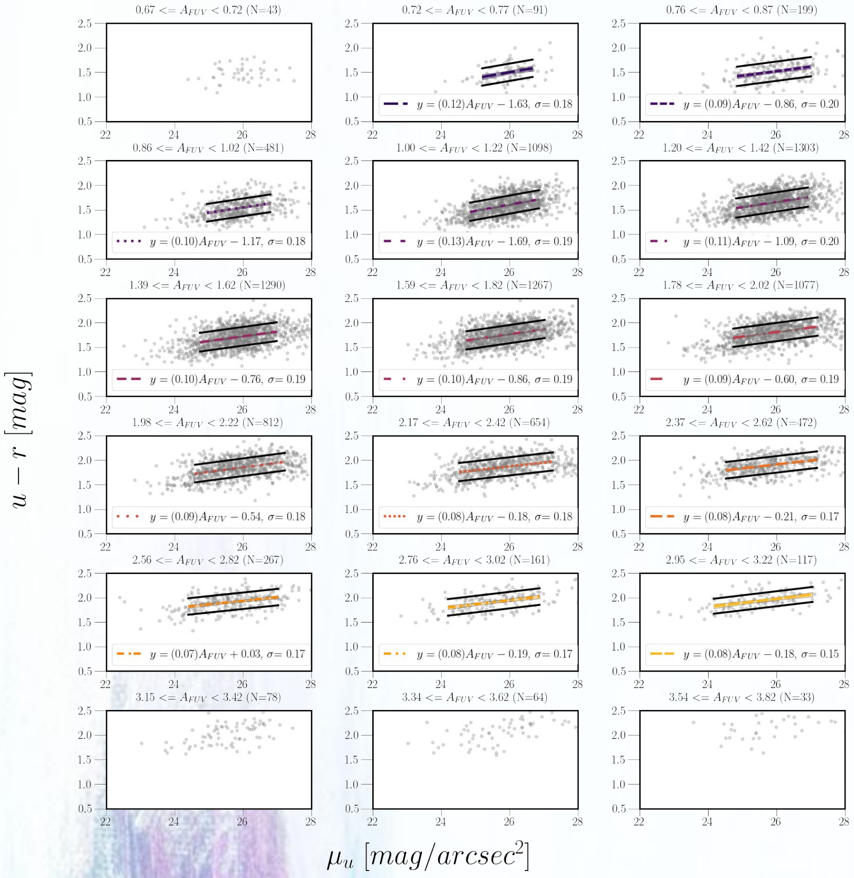

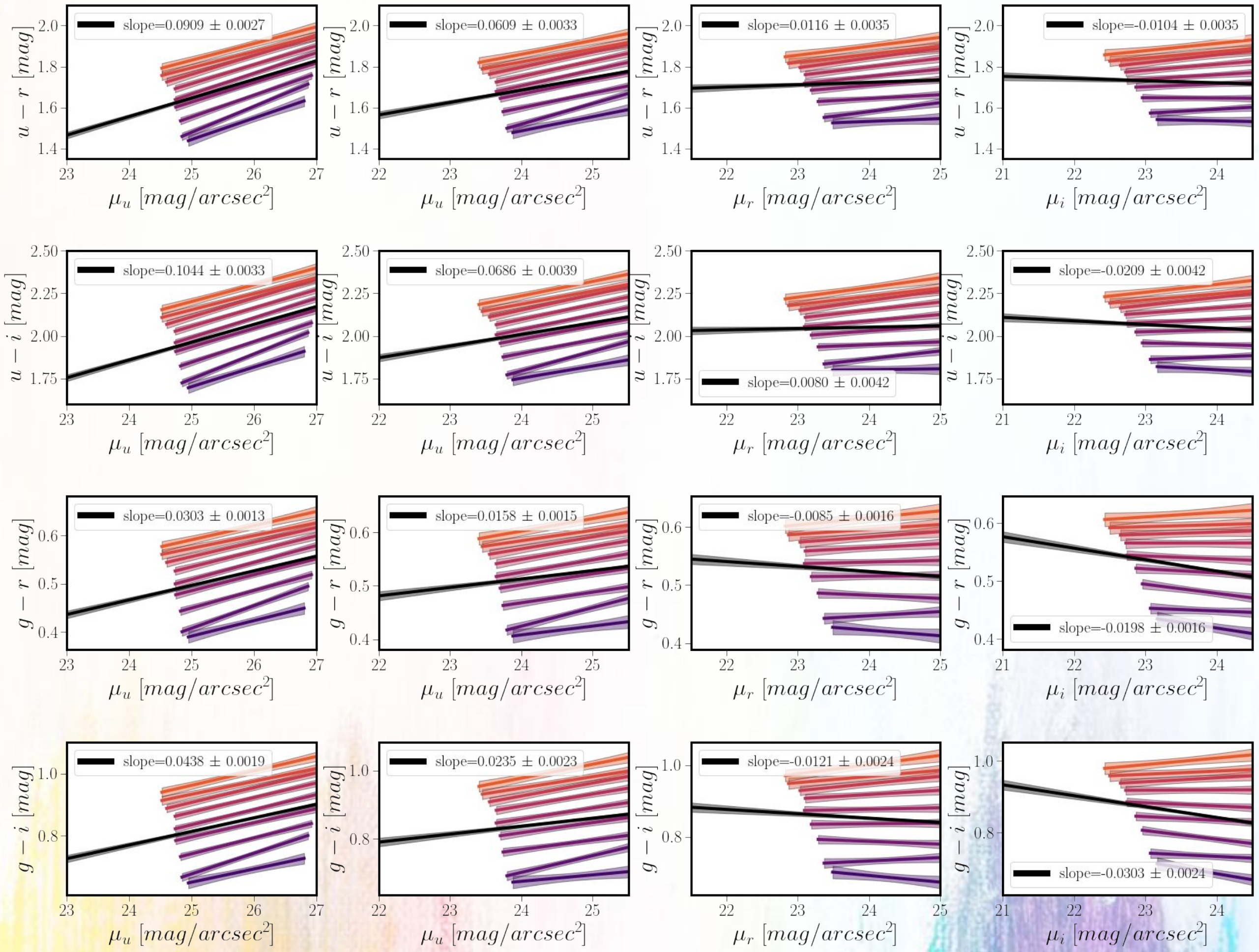
slope=0.0909 ± 0.0027
slope=0.0609 ± 0.0033
slope=0.0116 ± 0.0035
slope=-0.0104 ± 0.0035
slope=0.1044 ± 0.0033
slope=0.0686 ± 0.0039
slope=0.0080 ± 0.0042
slope=-0.0209 ± 0.0042
slope=0.0303 ± 0.0013
slope=0.0158 ± 0.0015
slope=-0.0085 ± 0.0016
slope=-0.0198 ± 0.0016
slope=0.0438 ± 0.0019
slope=0.0235 ± 0.0023
slope=-0.0121 ± 0.0024
slope=-0.0303 ± 0.0024
$u - r$ [mag]
$u - i$ [mag]
$g - r$ [mag]
$g - i$ [mag]
μ_u [mag/arcsec^2]
μ_r [mag/arcsec^2]
μ_i [mag/arcsec^2]